Bioelectrochemistry 145 (2022) 108071

Contents lists available at ScienceDirect

Bioelectrochemistry

journal homepage: www.elsevier.com/locate/bioelechem

Portable glucose biosensor based on polynorepinephrine@magnetite nanomaterial integrated with a smartphone analyzer for point-of-care application

Artur Jędrzak [a,b,*], Maria Kuznowicz [a], Tomasz Rębiś [c], Teofil Jesionowski [a]

[a] Institute of Chemical Technology and Engineering, Faculty of Chemical Technology, Poznan University of Technology, Berdychowo 4, Poznan PL-60965, Poland
[b] NanoBioMedical Centre, Adam Mickiewicz University, Wszechnicy Piastowskiej 3, Poznan PL-61614, Poland
[c] Institute of Chemistry and Technical Electrochemistry, Faculty of Chemical Technology, Poznan University of Technology, Berdychowo 4, Poznan PL-60965, Poland

ARTICLE INFO

Article history:
Received 29 November 2021
Received in revised form 31 December 2021
Accepted 14 January 2022
Available online 19 January 2022

Keywords:
Smartphone-based sensor
Glucose biosensor
Point-of-care testing
Polynorepinephrine
Screen-printed electrode

ABSTRACT

This work describes a novel nanoplatform based on polynorepinephrine (PNE) grafted on magnetite nanoparticles (Fe_3O_4) with glucose oxidase (GOx) from *Aspergillus niger* (Fe_3O_4@PNE-GOx). The system was integrated with a smartphone analyzer as a potential point-of-care testing (POCT) biosensor for glucose measurement.

Covering the magnetite surface with the biomimetic polymer polynorepinephrine significantly increased the effectiveness of enzyme immobilization which was 38.40 mg g^{-1}, compared with 17.30 mg g^{-1} on the bare surface of magnetite. The Fe_3O_4@PNE-GOx nanoplatform was deposited on a screen-printed electrode (SPE) and then used with the world's smallest ready-to-go potentiostat and a smartphone in tandem for glucose measurement. This biosensor displayed a broad range of linearity (0.2–24 mM), a low detection limit (6.1 μM), and good sensitivity (97.34 μA mM^{-1} cm^{-2}). Moreover, it exhibited a fast electrocatalytic response (8 s), and long-term stability (up to 20 weeks). It was used to detect glucose in real samples such as human serum, human blood, infusion fluid, and commercial glucose solutions.

The results obtained indicate that the proposed biosensor may be an attractive system for point-of-care testing (POCT), or in various industries, using a smartphone and potentiostat in tandem.

1. Introduction

Diabetes mellitus is a long-term illness that affects human life quality. This health issue is related to a lack of digestion of monosaccharides, especially glucose. The condition may have various causes: (i) non-production of insulin, a hormone responsible for the transfer of sugars from the blood to cells (type 1 diabetes); (ii) its resistance to monosaccharides (type 2 diabetes); or (iii) its blocking by placental hormones, increasing the blood sugar level in pregnant women (type 3, gestational diabetes) [1,2]. Persistently high glucose concentration in the blood may cause serious health problems such as kidney disease, heart disease, cancers, blindness, depression, dementia, and many others [3,4].

Therefore, glucose measurement is one of the most prominent analyses in clinical diagnostics, and it also plays a crucial role in pharmacy, environmental monitoring, and in the food industry, for the precise determination of the amount of glucose in products [5–7].

In 2021, the global biosensors market was worth US$ 25.5 billion, and it is projected to grow at a phenomenal 7.9% per year until reaching US$ 36 billion in 2027. Nearly half of the biosensor market is accounted for by medical biosensors, including electrochemical glucose biosensors [8].

However, due to many errors and limitations in commercial blood glucometers, caused by factors such as inappropriate storage, coding, calibration, the strip manufacturing process, and susceptibility to the influence of temperature on these devices, the U.S. Food and Drug Administration (FDA) has issued recommendations for new blood glucometers [9–11]. The primary implications of the new guidance for diabetes are that (i) newly produced glucose biosensors will need to be more accurate, (ii) larger studies will be required before they are authorized, and (iii) accuracy will be more prominently displayed on their packaging [12,13]. The FDA guidelines state that 95% of all measured values of glucose

* Corresponding author.
E-mail address: artur.jedrzak@put.poznan.pl (A. Jędrzak).

https://doi.org/10.1016/j.bioelechem.2022.108071
1567-5394/

in blood must be within 15% of the true value, and 99% should be within 20% of the true value [13].

Moreover, the increasingly widespread availability of modern technology such as smartphones, tablets, and smartwatches is leading to an increase in their use in human medical care [14–16]. Comprehensive digitization is driving the development of point-of-care testing (POCT). POCT, or bedside testing, is a type of medical diagnostic study performed at the place and time of care [17–19]. This trend is antagonistic to the traditional and complex system of testing only in a medical laboratory, which significantly prolonged the time of analysis and delayed the ability to treat the patient's condition. According to specialists, upcoming progress will affect therapy in the case of patients with diabetes, stroke, infectious diseases, and cancer [17–19].

This work concerns a proposed smartphone-based biosensor for quick, simple, and mobile glucose measurement, with the potential for use in diabetes care, as well as in the food and pharmaceutical industries [13,20]. Portable biosensors can be used in situations such as point-of-care diagnostics, with the added benefit of being able to operate in real time (as a mobile diagnostic station).

Our straightforward synthesis of a novel hybrid nanoplatform based on polynorepinephrine grafted onto magnetite nanoparticles (Fe_3O_4@PNE) with glucose oxidase (GOx) unveils a potential nanomaterial for the immobilization of enzymes as well as a platform for biosensors, compliant with the FDA guidelines. The proposed biosensor may be an attractive alternative for portable, rapid glucose measurement, with long-term stability for glucose detection in real samples such as human serum and blood. It is also significant that when this work was undertaken, there were no existing literature reports on this type of tandem system (potentiostat-smartphone) with hybrid nanomaterials based on magnetite@polynorepinephrine for glucose detection.

2. Reagents and apparatus

2.1. Materials and chemicals

Iron(II) chloride tetrahydrate ($FeCl_2{\cdot}4H_2O$), iron(III) chloride hexahydrate ($FeCl_3{\cdot}6H_2O$), and ammonia solution (25%), norepinephrine hydrochloride, phosphate buffer saline (PBS) (pH 7.4, 10 mM), citric buffer (pH 5.5, 10 mM), glucose oxidase from *Aspergillus niger* (protein content 65–85%, molecular weight 160 kDa), α-D-Glucose (≥99.5%, MW: 180.16 g mol^{-1}) (hydroxymethyl)ferrocene (HFc), tris(hydroxymethyl)aminomethane (TRIS), human serum from male AB plasma, fructose, maltose, sucrose, uric acid, ascorbic acid, L-cysteine, and dopamine were purchased from Merck, Poland. Human blood was purchased from Bio-Rad, USA. Biosensor systems were constructed based on a screen-printed electrode (SPE) obtained from Palmsens (Houten, Netherlands). All of the chemicals were of analytical grade quality.

2.2. Synthesis of Fe_3O_4@PNE hybrid material

The preparation of magnetite nanoparticles was based on the co-precipitation method. $FeCl_3{\cdot}6\,H_2O$ (3.44 g; 11.09 mM) and $FeCl_2{\cdot}4\,H_2O$ (1.72 g; 7.55 mM) were dissolved in 100 mL of Milli-Q® water, and heated to 90 °C. 20 mL of 25% aqueous ammonia was added dropwise, and synthesis was performed in a nitrogen gas atmosphere, which reduced the amount of oxygen in the system. The system was cooled to ambient temperature after 30 min.

To coat the nanoparticles with polynorepinephrine, 200 mL of TRIS buffer solution (pH 8.5, 10 mM) was added to 100 mg of the magnetite nanoparticles obtained in the previous step. The solution was sonicated to homogeneity, and then 100 mg of norepinephrine was added (0.87 mM). The process was conducted for different time intervals (2, 6, 24 h). The synthesis of the Fe_3O_4@PNE hybrid material is illustrated schematically in Fig. 1A.

2.3. Glucose oxidase immobilization on the Fe_3O_4@PNE nanoplatform

Glucose oxidase was immobilized on the surface of Fe_3O_4 or Fe_3O_4@PNE using an adsorption process, with the addition of 5 mg of the nanomaterial and 0.5 mg of glucose oxidase. The process was carried out in 1 mL citric buffer (10 mM, pH 5.5). To optimize the process, the immobilization was carried out over different time intervals (1, 2, 6, 10, 24, and 48 h). The immobilization process is illustrated schematically in Fig. 1B.

2.4. Fabrication of SPE/Fe_3O_4@PNE-GOx electrode

At the next stage, 1 μL of the obtained Fe_3O_4@PNE-GOx nanomaterial (6.18 mg mL^{-1}) was deposited on the surface of a screen-printed electrode (SPE) and left to dry at ambient temperature. The resulting system was ready to use for electrochemical testing. The electrode modification is shown schematically in Fig. 1C.

2.5. Physicochemical analysis

Transmission electron microscopy (TEM) analysis was carried out using a Jeol analyzer (JEM-1400) with a resolution of 2 nm and a maximum acceleration of 120 kV. The functional groups present in the structure of the hybrid platforms were determined using Fourier transform infrared spectroscopy (FTIR). The FTIR spectra were obtained using a Vertex 70 spectrometer. The nanomaterials were analyzed as tablets, made by combining 2 mg of the test substance with 250 mg of anhydrous KBr at a pressure of 10 MPa. Atomic force microscopy (AFM) was performed using an Agilent 5500 in intermittent contact mode, in atmospheric conditions. To test the stability of the materials in a liquid solvent, zeta potential (ζ) and polydispersity index (PdI) values were determined using a Zetasizer Nano ZS with a range of 0.6–6000 nm.

2.6. Electrochemical study

All electrochemical measurements were performed using the world's smallest potentiostat, the Sensit Smart (Palmsens, Netherlands) [21]. Electrochemical tests were carried out using the dedicated PStouch application. Different concentrations of glucose solution were dissolved in 10 mM PBS (pH 7.4) with 10 mM hydroxymethyl(ferrocene) and examined using cyclic voltammetry (CV) and chronoamperometry (CA). The potential was set between –0.2 and 0.6 V for CV testing, and the scanning rate was 10 mV s^{-1}. The constant potential for glucose detection by CA was set at 0.3 V. The repeatability of the glucose sensor was investigated by evaluating five separate electrodes. The sensor was stored in a refrigerator and tested every two weeks (for 20 weeks) to establish stability over time. The response of the biosensor in glucose detection was evaluated in the presence of potential interferents such as fructose, saccharose, maltose, L-cysteine, uric acid, ascorbic acid, and dopamine. Concentrations of the aforementioned interferents were 1 mM which is much higher than would normally be encountered in real samples. The biosensor was also used for glucose measurements in real samples such as human serum, human blood, infusion glucose solutions, and commercial glucose solutions. Additionally, real glucose solutions were tested using a commercial glucometer. All of these results are given in Table 5 (in section 3.6).

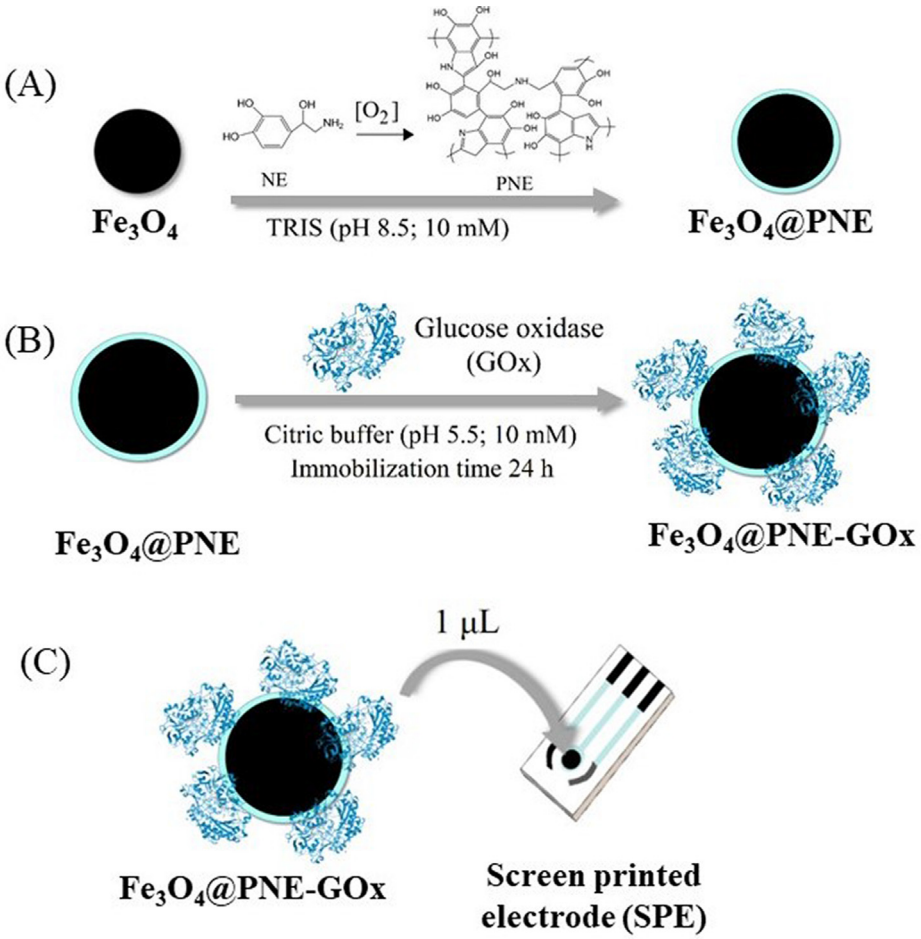

Fig. 1. Synthesis of magnetite@polynorepinephrine nanomaterial (A); immobilization of GOx on Fe_3O_4@PNE nanoplatform (B); modification of the screen-printed electrode (SPE) (C).

3. Results

3.1. Physicochemical characterization

The morphological structures of Fe_3O_4 and Fe_3O_4@PNE were investigated by transmission electron microscopy (TEM). The magnetite nanoparticles, as shown in Fig. 2A, present a uniformly spherical shape with diameters in the range 7–11 nm.

The Fe_3O_4 coated with a polynorepinephrine layer is visible in the second TEM image (Fig. 2B). The thickness of the PNE coating is uniform, of the order of 2–3 nm. The TEM images confirmed the presence of a thin, well-defined structure on the surface of the nanoparticles. FTIR and zeta potential analysis also validated the surface functionalization of the magnetite nanoparticles.

As compared to bare magnetite nanoparticles, PNE coating has a significant impact on the hydrodynamic particle size. The PdI and zeta potential values obtained for magnetite and for the Fe_3O_4@-PNE nanomaterial are summarized in Table 1. The magnetite nanoparticles had a dispersity of 0.195, which increased to 0.419 when they were coated with PNE. The zeta potential changed from

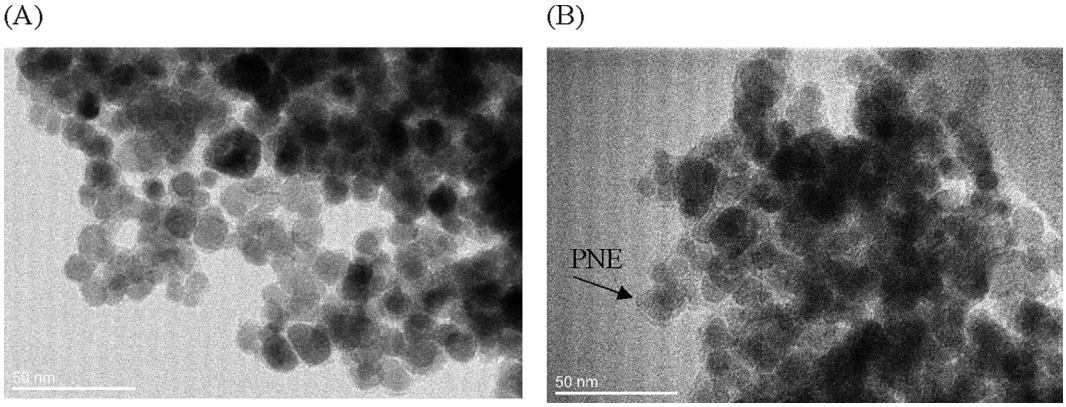

Fig. 2. Transmission electron microscopy (TEM) micrographs of the synthesized magnetite nanoparticles (A) and magnetite@polynorepinephrine nanomaterial (B).

Table 1
PdI and zeta potential analysis of Fe_3O_4 and Fe_3O_4@PNE (n = 3).

Sample	PdI	Zeta potential [mV]
Fe_3O_4	0.195 ± 0.032	−43.3 ± 0.5
Fe_3O_4@PNE	0.419 ± 0.020	−26.5 ± 0.8

–43.3 mV for Fe_3O_4 NPs to –26.5 mV for Fe_3O_4@PNE NPs, which may confirm that the surface is covered with a biopolymer. In addition, graphs of zeta potential distribution are provided in Fig. S1 (see Supplementary Material).

Fourier transform infrared spectroscopy (FTIR) tests were performed to analyze polynorepinephrine formation over time (2, 6, 24 h). Fig. 3 shows the FTIR spectra for Fe_3O_4 and Fe_3O_4@PNE formed at different polymerization times.

In the spectrum for Fe_3O_4, the visible strong peak at 577 cm^{-1} corresponds to vibrations of the Fe–O functional group [22]. Catechol groups (–OH) are associated with a large absorbance range of 3450–3100 cm^{-1} for PNE [23]. Overlapping C = C resonance vibrations and C–N stretching modes are associated with peaks at 1615 cm^{-1} and 1514 cm^{-1} respectively [24].

In addition, the increased intensity observed over time suggests that a greater amount of polynorepinephrine was formed after a longer polymerization time. These results demonstrate the efficiency of the PNE coating of magnetite nanoparticles (Fig. 3).

3.2. Immobilization of glucose oxidase(GOx)

The amount of immobilized GOx on the Fe_3O_4@PNE nanoplatform and the optimal conditions for this process were determined using the Bradford protein assay.

The immobilization process was also affected by the processing time (1, 2, 3, 6, 10, 24, 48 h) on the different nanoplatforms (Fe_3O_4 and Fe_3O_4@PNE) – these results are shown in Fig. S2 (see Supplementary Material). The highest amount of enzyme immobilized on both nanoplatforms was obtained after 24 h, and this was determined as the optimal time. The addition of PNE nanoparticles increases the amount of enzyme immobilized on the matrix surface more than twofold (the rates are 17.3 and 38.4 mg g^{-1} for Fe_3O_4 and Fe_3O_4@PNE hybrid nanomaterial, respectively).

It is caused by catechol groups occurring in the structure of polynorepinephrine, which present high reactivity towards nucleophiles like thiol, amino groups found in amino acids in the structure of the enzyme. The creation of hydrogen bonds between glucose oxidase (GOx) molecules and quinones, or the amino groups presented in the Fe_3O_4@PNE nanoplatform may explain the higher efficiency of GOx immobilization on the hybrid nanomaterial [25,26].

Additionally, interactions between enzyme (GOx) and nanomaterial (Fe_3O_4@PNE) may be based on van der Waals forces, ionic interactions or hydrogen bonds,

[27]. The results obtained are summarized in Table 2 and are compared with other carriers that have been used to immobilize glucose oxidase.

To characterize the morphology of the Fe_3O_4@PNE nanomaterial before and after the immobilization of glucose oxidase, images were taken using atomic force microscopy (AFM) (Fig. 4).

As shown in Fig. 4A, the 3D AFM images of Fe_3O_4@PNE presented well-formed nanoparticles, as was also confirmed by the related height profile (Fig. S3A; see Supplementary Material). Fig. 4B shows the Fe_3O_4@PNE-GOx surface, for which the value of the parameter *z* is more than doubled compared with the system without GOx (2.5 and 6.2 nm for Fe_3O_4@PNE and Fe_3O_4@PNE-GOx respectively).

The roughness coefficient (*Sa*) was also determined for the hybrid material before and after immobilization; the results obtained are given in Table 3 (n = 3).

The value of *Sa* for the material after immobilization is lower than the value for the matrix before GOx adsorption. This result confirms the smoothing effect of the enzyme.

3.3. Electrochemical tests of SPE/Fe_3O_4@PNE-GOx electrode

For electrochemical characterization of the analyzed systems, cyclic voltammograms of the bare screen-printed electrode (SPE), modified SPE/Fe_3O_4@PNE and SPE/Fe_3O_4@PNE-GOx electrodes were recorded in the presence of 1 mM $Fe(CN_6)^{3-/4-}$ (Fig. S4; see Supplementary Material). As shown in Fig. S4, a peak-to-peak separation of 150 mV was observed for the unmodified SPE electrode. Separations of 143 and 120 mV were recorded for the SPE/Fe_3O_4@PNE and SPE/Fe_3O_4@PNE-GOx electrodes respectively. These values indicate the irreversible behavior of $[Fe(CN)_6]^{3-/4-}$ at the studied electrodes. However, the decrease in peak-to-peak separation after electrode modification suggests the acceleration of charge transfer kinetics compared with the bare SPE. The deposition of nanostructured Fe_3O_4@PNE and Fe_3O_4@PNE-GOx materials on the surface of the SPE results in a significant increase in redox peak currents. The highest peak currents were observed for the SPE/Fe_3O_4@PNE-GOx electrode, and can be attributed to its having the highest electroactive surface area.

Electrochemical impedance spectroscopy (EIS) was next applied, to study the electron transfer characteristics. The EIS spectra are displayed in the inset of Fig. S5 as Nyquist plots, fitted with theoretically computed findings using an equivalent Randles cir-

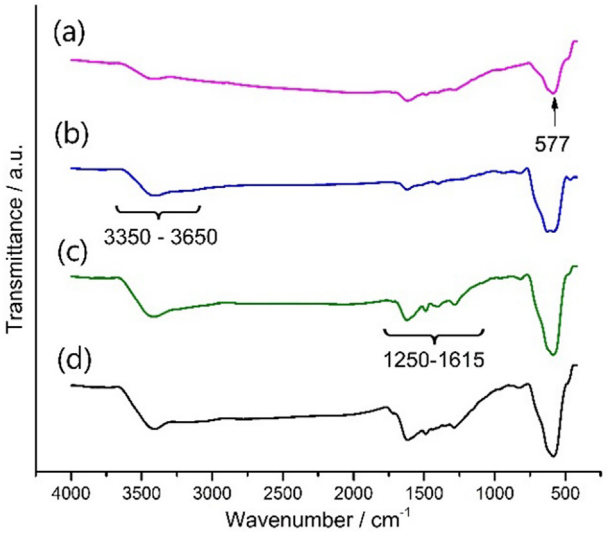

Fig. 3. Fourier transform infrared spectroscopy (FTIR) spectra obtained for Fe_3O_4 (a) and for Fe_3O_4@PNE formed at 2 h (b), 6 h (c), 24 h (d).

Table 2
Amounts of GOx immobilized on various platforms.

Sample	Immobilized GOx /mg g^{-1}	Ref
SiO_2/Lig	25.28	[25]
CNCs	20.08	[28]
OMC	37.38	[29]
YS-DMONs	20.10	[30]
Fe_3O_4/PDA	35.20	[31]
Fe_3O_4	17.30	This work
Fe_3O_4@PNE	38.40	This work

Cellulose nanocrystals (CNCs); ordered mesoporous carbon (OMC); yolk-shell tetrasulfide bond bridged dendritic MONs (YS-DMONs); silica-lignin (SiO_2/Lig), magnetite/polydopamine (Fe_3O_4/PDA)

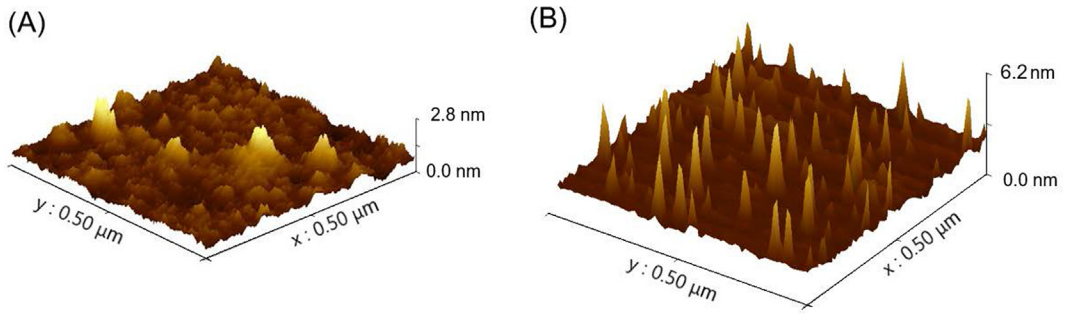

Fig. 4. AFM images of Fe_3O_4@PNE nanomaterial before GOx immobilization (A) and after GOx immobilization (B).

Table 3
Coefficient of roughness (*Sa*).

Sample	Fe_3O_4@PNE	Fe_3O_4@PNE -GOx
Sa	61.21 ± 2.44	81.21 ± 2.66

cuit model. The charge transfer resistance (R_{ct}) can be calculated from the semicircle obtained in the Nyquist plot. The plots show that the R_{ct} of the bare SPE (ΔR_{ct} = 2350 Ω) is significantly decreased by coating with Fe_3O_4@PNE (ΔR_{ct} = 86 Ω), suggesting the facilitation of the electron transfer kinetics by Fe_3O_4@PNE nanoparticles at the SPE surface. The immobilization of GOx on Fe_3O_4@PNE caused an increase from 86 Ω to 114 Ω, which may be due to the insulating nature of GOx. It should be noted that at pH above 4.2 (the isoelectric point) GOx exists in a negatively charged form [32]. This may cause repulsion between the anionic $Fe(CN)_6^{3-}/Fe(CN)_6^{4-}$ redox probes and the negative charge carried by GOx, resulting in a slightly larger semicircle diameter, and thus indicating an increase in resistance compared with SPE/Fe_3O_4@-PNE. Similarly, the extensive protein caging of GOx's FAD redox center confirmed a reduction in electron transfer [33].

The effective surface areas of the SPE, SPE/Fe_3O_4@PNE, and SPE/Fe_3O_4@PNE-GOx electrodes were calculated from the voltammetric peak currents recorded in a solution containing 1 mM of Fe $(CN_6)^{3-/4-}$ at scan rates ranging from 10 to 100 mV s^{-1} (Fig. S6; see Supplementary Material) using the Randles–Sevcik equation [34]:

$$I_p = \left(2.69 \cdot 10^5\right) nACD^{\frac{1}{2}} v^{\frac{1}{2}} \quad (1)$$

where n is the number of electrons engaged in the redox reaction (n = 1), A is the electrode surface area (cm^2), C is the concentration of the redox species in solution (0.01 mol cm^{-3}), D is the molecule's diffusion coefficient in solution ($7.6 \cdot 10^{-6}$ cm^2 s^{-1}), and v is the scan rate (V s^{-1}) [35,36].

The effective surface areas calculated for SPE, SPE/Fe_3O_4@PNE and SPE/Fe_3O_4@PNE-GOx were high values of 0.078 cm^2, 0.300 cm^2 and 0.284 cm^2 respectively. The rise in current intensity may thus be linked to the nanoelectrodes' increased surface area [34].

Next, the electrochemical properties of the SPE/Fe_3O_4@PNE-GOx material were studied in the presence of HFc redox mediator. The effect of various scan rates on the electrochemical properties is depicted in Fig. 5A. The redox current increased as the scan rate was increased from 10 to 100 mV s^{-1}. The dependence of the current (I_p) on the square root of the scan rate ($v^{1/2}$) (Fig. 5B) is an important diagnostic criterion when using cyclic voltammetry to determine the type of reaction mechanism. The results indicate that the redox reaction of GOx on the electrode surface is a quasi-reversible diffusion-controlled electrochemical operation [37].

In addition, polynorepinephrine has numerous catechol groups which are functional redox ligands, which are responsible for electron hopping transfer which mimics electron transport in a biological system, and redox polymers [38].

Electrochemical investigations were performed to characterize the response of the Fe_3O_4@PNE-GOx electrode. Cyclic voltammograms (CVs) were obtained without glucose and in the presence of glucose, in a range from –0.2 V to 0.6 V, at a scan rate of 10 mV s^{-1} (Fig. 6A). The Fe_3O_4@PNE-GOx biosensor catalyzes the oxidation of glucose in the presence of an external redox mediator (HFc). At sufficiently positive potential the reduced form of the mediator HFc is converted to its catalytically active oxidized form HFc^+. Then electron exchange occurs between $FADH_2$ and HFc^+, resulting in the regeneration of FAD and the formation of HFc. The re-oxidation of HFc on the electrode surface results in a bioelectrocatalytic response that is proportional to the quantity of glucose present in the solution [39–41]. The reactions occurring can be presented as follows:

$$\text{glucose} + \text{FAD} \rightarrow \text{gluconolactone} + FADH_2 \quad (2)$$

$$FADH_2 + 2\,HFc^+ \rightarrow FAD + 2\,HFc + 2H^+ \quad (3)$$

$$HFc \rightarrow HFc^+ + e^- \quad (4)$$

In Fig. 6B, the curve presents the correlation between peak current and glucose concentration. The voltammetric response approached saturation when the glucose concentration was above 110 mM. This response is a result of Michael–Menten kinetics and is typical of enzymatic biosensors [42].

The relationship between the response current and glucose concentration can be found using Lineweaver–Burk plots. The K_m^{app} value of 1.35 mM, reflecting the affinity of the enzyme to the electrode, is smaller than previously reported values of 2.10, 3.44, 10.11, and 14.50 mM [43–46], indicating that the GOx immobilized on Fe_3O_4@PNE has a high affinity to glucose.

Following optimization of the settings, the biosensing system's analytical response was assessed using chronoamperometry, in which different quantities of glucose were sequentially injected and continuously stirred into PBS (pH 7.4) supplemented with 10 mM of HFc, and with a potential of 0.3 V. The analytical performance of the prepared Fe_3O_4@PNE-GOx biosensor was evaluated with glucose concentrations varying from 0.2 to 34 mM (Fig. 7A). The linear relation of the current with concentrations of glucose between 0.2 mM and 24 mM, with a correlation coefficient of 0.998 (n = 3), is shown in Fig. 7B. Based on the slope of the linear fit in Fig. 7B, the sensitivity of the biosensor was calculated as 97.34 µA mM^{-1}. The obtained calibration curve enables the testing of glucose levels from hypoglycemia (<3.8 mM/L) through normal glucose levels (3.9–5.5 mM), early diabetes (5.6–10.0 mM), and diabetes (greater than10.0 mM).

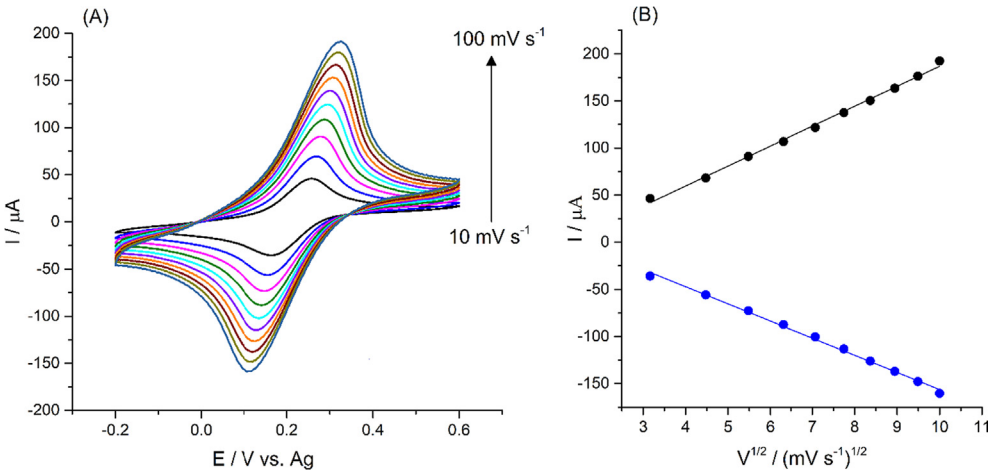

Fig. 5. Cyclic voltammograms of SPE/Fe_3O_4@PNE-GOx in PBS containing 10 mM hydroxymethyl(ferrocene) at different scan rates (in the range from 10 to 100 mV s^{-1}) (A); linear fitting chart of the I_{pa} (y = 21.189x – 25.049, R^2 = 0.996) and I_{pc} (y = -18.204x + 25.756, R^2 = 0.997) versus $v^{1/2}$ (B).

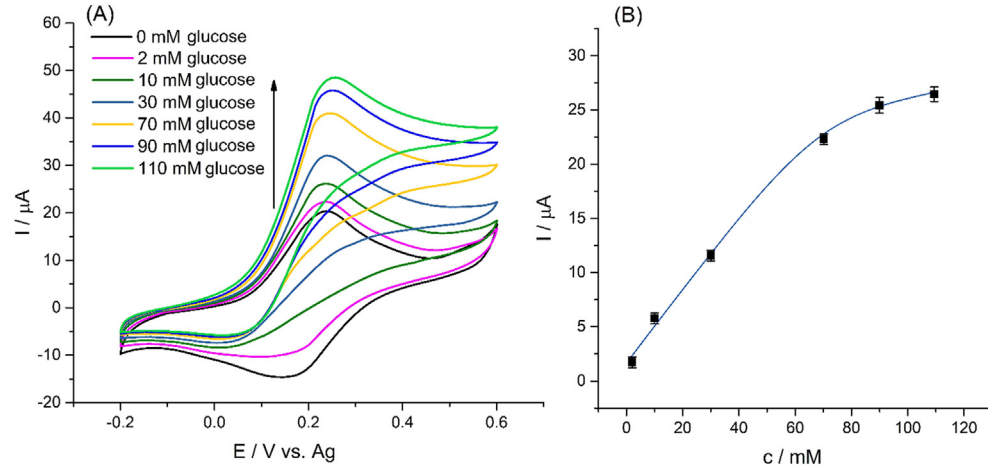

Fig. 6. Cyclic voltammograms of Fe_3O_4@PNE-GOx electrode in PBS solution containing 10 mM HFc and various concentrations of glucose at scan rate 10 mV s^{-1} (A); calibration graph (B) (n = 3).

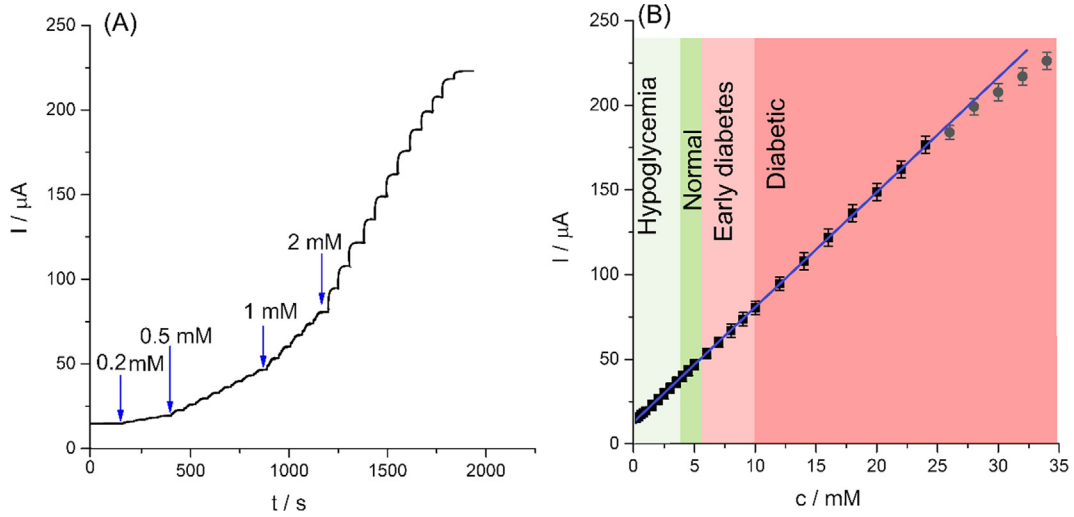

Fig. 7. Chronoamperometric response of SPE/Fe_3O_4@PNE-GOx electrode in 10 mM PBS (pH 7.4) containing 10 mM of HFc on injection of various concentrations of glucose at a working potential of 0.3 V (A); the resulting calibration curve (y = 6.814x + 12.662, R^2 = 0.998) (B).

The presented calibration curves are adequate for calculating glucose concentrations in both healthy and diabetic patients [47]. The limit of detection (LOD) of the SPE/Fe_3O_4@PNE-GOx electrode was calculated as 6.1 μM, using the following equation:

$$LOD = 3 \cdot \frac{\delta}{S} \quad (5)$$

where S is the slope of the calibration curve and δ is the standard deviation at the lowest concentration [48].

One of the characteristics of a biosensor is the response time, defined as the time required to achieve a 95% steady-state signal [49]. On exposure to a 2 mM glucose solution (Fig. S7; see Supplementary Material) the SPE/Fe_3O_4@PNE-GOx biosensor attained 95% of the constant signal after 8 s, which is faster than previously reported [50,51].

Without the use of mixing conditions, accurate measurements were obtained with the chronoamperometry method. Fig. 8A presents chronoamperometric responses of the SPE-based biosensor to different concentrations of glucose ranging from 0.5 to 22 mM at a working potential of 0.3 V. A well-defined amperometric response of the biosensor to successive additions of glucose was observed. The calibration curve was created using data from three runs and the average current response of the sensor after 45 s. Error bars represent the standard deviations of the measurements for each concentration. As shown in Fig. 8B, the linear range of the Fe_3O_4@PNE-GOx biosensor was from 0.5 to 22 mM of glucose, with a correlation coefficient of 0.996. Based on the slope of the linear fit in Fig. 8B, the sensitivity of the biosensor was calculated as 30.73 μA mM^{-1} cm^{-2}.

As shown in Table 4, the linear concentration range, limit of detection, and sensitivity are equivalent to those reported in the literature for enzyme biosensors.

3.4. Optimization of the SPE/Fe_3O_4@PNE-GOx electrode

The designed SPE/Fe_3O_4@PNE-GOx electrochemical sensor was optimized for several parameters, including temperature, pH of the solution, mediator concentration, and immobilization time. These parameters were adjusted in the presence of 2 mM glucose solution, always changing one parameter to obtain the optimum process conditions.

The pH value has a strong influence on the activity of the enzyme [61]. The influence of pH on the performance of the SPE/Fe_3O_4@PNE-GOx electrode was investigated (Fig. S8A; see Supplementary Material). The highest currents were observed for a pH of 7.4, and the electrode exhibited a good relative response in the pH range from 5.0 to 9.0. The optimal pH value determined in this test has been confirmed in other studies using glucose oxidase as the enzyme [31,62,63].

To evaluate the influence of temperature on the proposed system, tests were carried out for various temperatures in a range from 15 °C to 60 °C. The effect of temperature on the electrode response is shown in Fig. S8B. The highest currents were recorded at 40 °C; however, because the enzyme also showed high activity at 25 °C, this temperature was selected for subsequent experiments.

The glucose response with HFc (in the concentration range from 1 mM to 30 mM) is presented in Fig. S8C. Above 10 mM there was only a slight increase in the relative sensor response. Therefore, 10 mM HFc was used in further tests.

The effect of the immobilization time (2, 5, 10, 24, and 48 h) on the electrode response in the presence of 2 mM glucose is shown in Fig. S8D. The highest response was recorded for 24 h of immobilization, which confirms the results obtained with the Bradford method.

3.5. Interference tests

The selectivity of the prepared biosensor was investigated in the presence of interferents such as ascorbic acid, dopamine, uric acid, L-cysteine, and other sugars (saccharose, fructose, and maltose) by amperometric analysis at 0.3 V. The results (Fig. 9) showed that the current value did not vary appreciably in the presence of the above interferents. The experiments were carried out under previously determined optimal operating conditions (25 °C, 10 mM HFc, pH 7.4). However, the tested interferent concentrations are about 5 times higher than those found in blood [64].

Analysis of these results shows that the proposed system offers very high selectivity. At the same time, a very good response to glucose alone is retained, and the presence of interferents in the solution did not affect the glucose response.

3.6. Testing in real glucose samples

The glucose content in samples of human serum and human blood was measured, to demonstrate the practicality of the glucose sensor as a potential POCT biosensor. Measurements of known glucose concentrations in human serum samples were also performed to confirm the selectivity and sensitivity of the glucose measurement. Three different quantities of glucose (2.3 mM, 5.6 mM, 10.2 mM) were measured in human serum. The recovery was com-

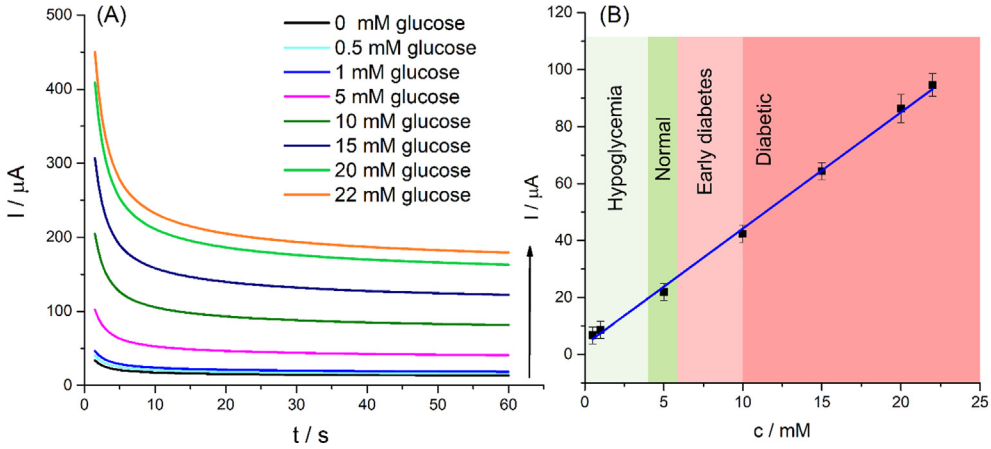

Fig. 8. Amperometric response of biosensors to different glucose concentrations without mixing conditions, containing 10 mM of HFc at a working potential of 0.3 V (A); the resulting calibration curve (y = 4.043x + 4.392. R^2 = 0.996) (B).

Table 4
Comparison of the analytical performance of various glucose biosensors.

Electrode	Sensitivity (μA mM^{-1} cm^{-2})	LOD (μM)	Linear range (mM)	References
GOx-SiO_2/Lig	0.78	145.00	0.5–9.0	[25]
Fe_3O_4/PDA-GOx	1.55	115.74	1–26.0	[31]
ZnO/Pt/GCSPs/GOx	88.36	0.03	0.05–1.0	[52]
GOx/Graphene/CHIT/GCE	37.93	0.02	0.08–12.0	[53]
Graphene–CdS–GOx	1.76	700.00	2.0–16.0	[54]
GOx/Ag@MWCNT-IL-Fe_3O_4	–	2.12	0.006–2.0	[55]
GOx/Au/MXene/Nafion	4.20	5.90	0.1–18.0	[56]
GOx/Au/MWCNTs/PVA	16.60	200.00	0.5–8.0	[57]
GOx/AuNPs/Pty/PB	16.70	1.00	0.00001–1.0	[58]
PNE/GOD/AuNPs@PNE/Au	35.40	1.34	0.003–3.4	[59]
Nafion/GOx/ZnO/Au	24.60	5.00	0.1–7.1	[60]
Fe_3O_4@PNE-GOx	97.30	6.10	0.2–24.0	This work

Glucose oxidase (GOx/GOD); zinc oxide (ZnO); platinum (Pt); chitosan submicron particles (GCSPs); chitosan (CHIT); cadmium sulfide nanoparticle (CdS); silver (Ag); multi-walled carbon nanotubes (MWCNT); gold (Au); magnetite (Fe_3O_4); polyvinyl alcohol (PVA); polydopamine (PDA); lignin (Lig); silica (SiO_2); Prussian blue (PB); polytyramine layer (Pty); molybdenum disulfide (MoS_2)

Table 5
Measurement of human blood, human serum, infusion glucose and glucose samples (n = 3), using our proposed SPE/Fe_3O_4@PNE-GOx biosensor and a commercial glucometer.

Sample	Glucose concentration / mM	SPE/Fe_3O_4@PNE-GOx		Commercial glucometer	
		Found / mM	Recovery / %	Found / mM	Recovery / %
human serum	0	0	–	0	–
	2.3	2.2 ± 0.1	95.7	2.1 ± 0.1	91.3
	5.6	5.4 ± 0.1	96.4	5.3 ± 0.1	94.6
	10.2	9.9 ± 0.1	97.1	9.6 ± 0.2	94.1
human blood	3.1	3.0 ± 0.1	96.8	2.7 ± 0.1	87.1
	6.1	6.0 ± 0.1	98.4	5.8 ± 0.2	95.1
	14.7	14.4 ± 0.2	98.0	13.9 ± 0.2	94.6
infusion fluid	5.7	5.6 ± 0.1	98.2	5.4 ± 0.3	94.7
glucose sample 1	4.4	4.3 ± 0.1	97.7	4.2 ± 0.3	95.4
glucose sample 2	5.5	5.3 ± 0.1	96.4	5.1 ± 0.2	92.7
glucose sample 3	7.8	7.5 ± 0.1	96.2	7.3 ± 0.2	93.6

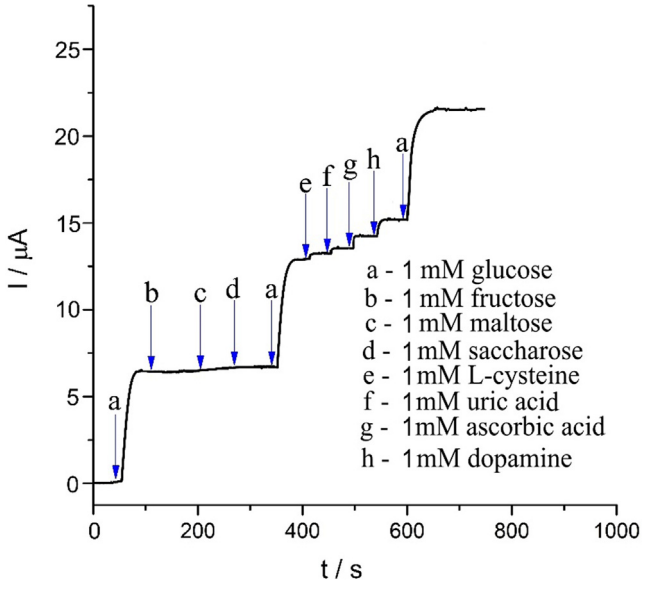

Fig. 9. Interference tests of the biosensor with 1 mM glucose, 1 mM fructose, 1 mM saccharose, 1 mM maltose, 1 mM L-cysteine, 1 mM uric acid, 1 mM ascorbic acid, and 1 mM dopamine in 10 mM HFc at 0.3 V.

puted at between 96% and 97% (n = 3), as shown in Table 5, demonstrating that the biosensor is also reliable for biological samples, and these results also confirmed its clinical usefulness. The Fe_3O_4@PNE-GOx modified electrode was tested in real sample analysis using the standard addition procedure. Subsequently, tests were carried out on human blood solutions with low, medium, and high glucose concentrations.

Finally, glucose concentrations were also determined in commercially available glucose samples, including infusion fluids and glucose drinks. The results indicated good accuracy in the measurement of glucose, with recoveries between 96.1% and 97.7% for our proposed SPE/Fe_3O_4@PNE-GOx biosensor. The results demonstrate the electrochemical biosensor's good performance in the examination of genuine samples.

3.7. Storage stability and reproducibility of the biosensor

One of the major limitations of biosensors is their stability over time. The stability of the SPE/Fe_3O_4@PNE-GOx biosensor was tested over 20 weeks, with the sensor stored at 4 °C when not in use. Results indicating the electrode's stability over time are shown in Fig. 10.

The data show that current continues to flow through the electrode as time elapses, and the increases in intensity are proportional to the amount of glucose added. The current intensity for the same glucose additions decreases over time. However, the electrode retains more than 82.2% of its initial performance after 16 weeks, and 75.1% after 20 weeks. Its aging can be attributed to the progressive breakdown of the enzyme on the working electrode; the effect of other environmental variables (evaporation, contamination, oxidation, etc.) can be assumed to be limited or absent, because the biosensors were individually vacuum packaged before storage at elevated temperatures, and were used only once [64].

The stability of the sensor was also tested in terms of the number of tests performed, with the use of cyclic voltammetry. The curve was recorded in the presence of PBS (pH 7.4) together with

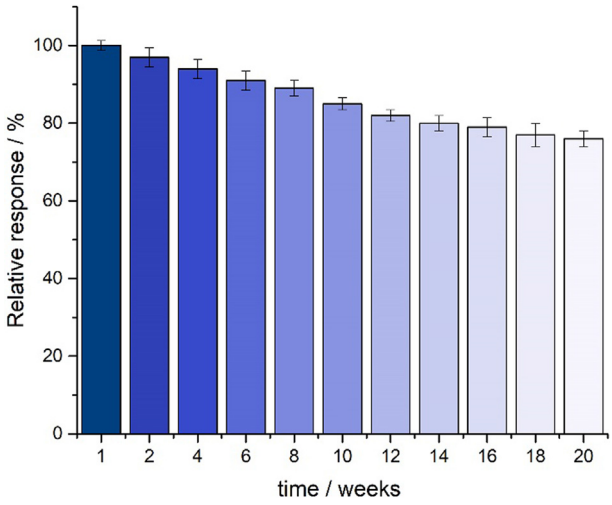

Fig. 10. SPE/Fe_3O_4@PNE-GOx biosensor relative response over time for 2 mM of glucose (n = 3).

10 mM hydroxymethyl(ferrocene) and 2 mM glucose. As shown in Fig. S9 (see Supplementary Material), after 100 scans, the sensor current response decreased to 89% of its original value, demonstrating the good stability of the proposed system.

Chronoamperometry was used to test the biosensor's repeatability and reproducibility, based on the addition of 2 mM of glucose to PBS (10 mM, pH = 7.4). The relative standard deviation (RSD) obtained (n = 5) was 3.1%, indicating high repeatability (inter-day assay). The intra-day assay value was 0.6%, indicating that the detection procedure is repeatable.

4. Conclusion

Herein, this work presents a smartphone-based biosensor for quick, simple, and mobile glucose measurement. The use of polynorepinephrine for coating magnetite nanoparticles allowed to improve the adsorption of enzyme onto the magnetite@polynorepinephrine hybrid nanoplatform. Furthermore, designing and obtaining the inorganic/organic carrier made it possible to obtain a synergistic effect to create a biosensor with improved properties such as sensitivity, selectivity, linear range and stability over time, as well as its possible to miniaturization and operation with a potentiostat and a smartphone in tandem.

Moreover, the proposed SPE/Fe_3O_4@PNE-GOx biosensor was characterized by selective glucose recognition and fast response in real glucose samples such like human blood, human serum, infusion fluids and commercial glucose samples. The proposed smartphone-based SPE/Fe_3O_4@PNE-GOx biosensor has the potential for use as a mobile, highly sensitive, highly selective instrument for rapid glucose measurements in medicine, in line with the trend toward point-of-care testing, as well as in various industries. Due to these properties, the obtained biosensor may be used as a portable analytical station having the advantage of being able to work in real-time, in conditions outside of the laboratory as a mobile diagnostic station.

Declaration of Competing Interest

The authors declare that they have no known competing financial interests or personal relationships that could have appeared to influence the work reported in this paper.

Acknowledgments

This work was financed and prepared as part of a research project supported by the National Science Centre Poland, no. 2017/27/B/ST8/01506.

Appendix A. Supplementary material

Supplementary data to this article can be found online at https://doi.org/10.1016/j.bioelechem.2022.108071.

References

[1] Y. Liu, Q. Yu, X. Luo, L. Yang, Y. Cui, Continuous monitoring of diabetes with an integrated microneedle biosensing device through 3D printing, Microsyst. Nanoeng. 7 (2021) 75, https://doi.org/10.1038/s41378-021-00302-w.
[2] A.T. Kharroubi, Diabetes mellitus: the epidemic of the century, World J. Diabetes 6 (6) (2015) 850, https://doi.org/10.4239/wjd.v6.i6.850.
[3] S. Moreno-Fernández, M. Garcés-Rimón, G. Vera, J. Astier, J.F. Landrier, M. Miguel, High fat/high glucose diet induces metabolic syndrome in an experimental rat model, Nutrients 10 (2018) 1–15, https://doi.org/10.3390/nu10101502.
[4] S.E. Capes, D. Hunt, K. Malmberg, H.C. Gerstein, Stress hyperglycaemia and increased risk of death after myocardial infarction in patients with and without diabetes: a systematic overview, Lancet 355 (9206) (2000) 773–778, https://doi.org/10.1016/S0140-6736(99)08415-9.
[5] S. Pakapongpan, R.P. Poo-arporn, Self-assembly of glucose oxidase on reduced graphene oxide-magnetic nanoparticles nanocomposite-based direct electrochemistry for reagentless glucose biosensor, Mater. Sci. Eng. C 76 (2017) 398–405, https://doi.org/10.1016/j.msec.2017.03.031.
[6] G. Emir, Y. Dilgin, A. Ramanaviciene, A. Ramanavicius, Amperometric nonenzymatic glucose biosensor based on graphite rod electrode modified by Ni-nanoparticle/polypyrrole composite, Microchem. J. 161 (2021) 105751, https://doi.org/10.1016/j.microc.2020.105751.
[7] T. Kong, Y. Chen, Y. Ye, K. Zhang, Z. Wang, X. Wang, An amperometric glucose biosensor based on the immobilization of glucose oxidase on the ZnO nanotubes, Sens. Actuators B Chem. 138 (1) (2009) 344–350, https://doi.org/10.1016/j.snb.2009.01.002.
[8] Report of Global Biosensors Market (2021 to 2026) – Increasing use of biosensors to monitor glucose levels in individuals with diabetes is driving growth, Dublin, April 2021
[9] M. Pohanka, Glucose electrochemical biosensors: The past and current trends, Int. J. Electrochem. Sci. 16 (2021) 1–12, https://doi.org/10.20964/2021.07.52.
[10] M.H. Hassan, C. Vyas, B. Grieve, P. Bartolo, Recent advances in enzymatic and non-enzymatic electrochemical glucose sensing, Sensors 21 (2021) 4672, https://doi.org/10.3390/s21144672.
[11] A.C. Carpenter, I.T. Paulsen, T.C. Williams, Blueprints for biosensors: design, limitations, and applications, Genes 9 (2018) 375, https://doi.org/10.3390/genes9080375.
[12] Healthline FDA updates guidelines on glucose meter accuracy. https://www.healthline.com/diabetesmine/fda-finalizes-meter-accuracy-rules#1., (n.d.).
[13] H. Zhang, W. Zhang, A. Zhou, in: Smartphone Based Medical Diagnostics, Elsevier, 2020, pp. 45–65, https://doi.org/10.1016/B978-0-12-817044-1.00004-1.
[14] V.B. Juska, M.E. Pemble, A critical review of electrochemical glucose sensing: evolution of biosensor platforms based on advanced nanosystems, Sensors 20 (2020) 1–28, https://doi.org/10.3390/s20216013.
[15] D. Ji, L. Liu, S. Li, C. Chen, Y. Lu, J. Wu, Q. Liu, Smartphone-based cyclic voltammetry system with graphene modified screen printed electrodes for glucose detection, Biosens. Bioelectron. 98 (2017) 449–456, https://doi.org/10.1016/j.bios.2017.07.027.
[16] J. Tran, R. Tran, J.R. White, Smartphone-based glucose monitors and applications in the management of diabetes: an overview of 10 salient "apps" and a novel smartphone-connected blood glucose monitor, Clin. Diabetes 30 (2012) 173–178, https://doi.org/10.2337/diaclin.30.4.173.
[17] E.I. Tzianni, J. Hrbac, D.K. Christodoulou, M.I. Prodromidis, A portable medical diagnostic device utilizing free-standing responsive polymer film-based biosensors and low-cost transducer for point-of-care applications, Sens. Actuators B Chem. 304 (2020) 127356, https://doi.org/10.1016/j.snb.2019.127356.
[18] D. Quesada-González, A. Merkoçi, Nanomaterial-based devices for point-of-care diagnostic applications, Chem. Soc. Rev. 47 (13) (2018) 4697–4709, https://doi.org/10.1039/c7cs00837f.
[19] J. Howick, J.W.L. Cals, C. Jones, C.P. Price, A. Plüddemann, C. Heneghan, M.Y. Berger, F. Buntinx, J. Hickner, W. Pace, T. Badrick, A. van den Bruel, C. Laurence, H.C. van Weert, E. van Severen, A. Parrella, M. Thompson, Current and future use of point-of-care tests in primary care: An international survey in Australia, Belgium, The Netherlands, the UK and the USA, BMJ Open. 4 (2014) 005611. https://doi.org/10.1136/bmjopen-2014-005611
[20] C. Florkowski, A. Don-Wauchope, N. Gimenez, K. Rodriguez-Capote, J. Wils, A. Zemlin, Point-of-care testing (POCT) and evidence-based laboratory medicine (EBLM)—does it leverage any advantage in clinical decision making?, Rev Clin

Lab Sci 54 (7-8) (2017) 471–494, https://doi.org/10.1080/10408363.2017.1399336.
[21] https://www.palmsens.com/product/sensit-smart
[22] Y. Wang, S. Wang, H. Niu, Y. Ma, T. Zeng, Y. Cai, Z. Meng, Preparation of polydopamine coated Fe_3O_4 nanoparticles and their application for enrichment of polycyclic aromatic hydrocarbons from environmental water samples, J. Chromatogr. A 1283 (2013) 20–26, https://doi.org/10.1016/j.chroma.2013.01.110.
[23] J. Chen, R.P. Liang, X.N. Wang, J.D. Qiu, A norepinephrine coated magnetic molecularly imprinted polymer for simultaneous multiple chiral recognition, J. Chromatogr. A 1409 (2015) 268–276, https://doi.org/10.1016/j.chroma.2015.07.052.
[24] S.M. Kang, S. Park, D. Kim, S.Y. Park, R.S. Ruoff, H. Lee, Simultaneous reduction and surface functionalization of graphene oxide by mussel-inspired chemistry, Adv. Funct. Mater. 21 (1) (2011) 108–112, https://doi.org/10.1002/adfm.201001692.
[25] A. Jędrzak, T. Rębiś, Ł. Klapiszewski, J. Zdarta, G. Milczarek, T. Jesionowski, Carbon paste electrode based on functional GOx/silica-lignin system to prepare an amperometric glucose biosensor, Sens. Actuators B Chem. 256 (2018) 176–185, https://doi.org/10.1016/j.snb.2017.10.079.
[26] J.G. Rivera, P.B. Messersmith, Polydopamine-assisted immobilization of trypsin onto monolithic structures for protein digestion, J. Sep. Sci. 35 (12) (2012) 1514–1520, https://doi.org/10.1002/jssc.201200073.
[27] H. Suo, M. Li, R. Liu, L. Xu, Enhancing bio-catalytic performance of lipase immobilized on ionic liquids modified magnetic polydopamine, Colloids Surf. B 206 (2021) 111960, https://doi.org/10.1016/j.colsurfb.2021.111960.
[28] Y.C. Yee, R. Hashim, A.R. Mohd Yahya, Y. Bustami, Colorimetric analysis of glucose oxidase-magnetic cellulose nanocrystals (CNCS) for glucose detection, Sensors 19 (2019) 2511, https://doi.org/10.3390/s19112511.
[29] X. Yang, W. Yuan, D. Li, X. Zhang, Study on an improved bio-electrode made with glucose oxidase immobilized mesoporous carbon in biofuel cells, RSC Adv. 6 (29) (2016) 24451–24457, https://doi.org/10.1039/c5ra27111h.
[30] Y. Yang, Y. Lu, P.L. Abbaraju, I. Azimi, C. Lei, J. Tang, M. Jambhrunkar, J. Fu, M. Zhang, Y. Liu, C. Liu, C. Yu, Stepwise degradable nanocarriers enabled cascade delivery for synergistic cancer therapy, Adv. Funct. Mater. 28 (28) (2018) 1800706, https://doi.org/10.1002/adfm.201800706.
[31] M. Kuznowicz, A. Jędrzak, T. Rębiś, T. Jesionowski, Biomimetic magnetite/polydopamine/β-cyclodextrins nanocomposite for long-term glucose measurements, Biochem. Eng. J. (2021) 108127, https://doi.org/10.1016/j.bej.2021.108127.
[32] E.J. Calvo, R. Etchenique, L. Pietrasanta, A. Wolosiuk, C. Danilowicz, Layer-by-layer self-assembly of glucose oxidase and os(Bpy)2ClPyCH$_2$NH-poly (allylamine) bioelectrode, Anal. Chem. 73 (2001) 1161–1168, https://doi.org/10.1021/ac0011686.
[33] F. Patolsky, G. Tao, E. Katz, I. Willner, Preliminary note C 60-mediated bioelectrocatalyzed oxidation of glucose with glucose oxidase, J. Electroanal. Chem. 454 (1-2) (1998) 9–13, https://doi.org/10.1016/S0022-0728(98)00257-5.
[34] I.C. Lekshmi, I. Rudra, R. Pillai, C. Sarika, M.S. Shivakumar, C. Shivakumara, S.B. Konwar, B. Narasimhamurthy, Enhanced catechol biosensing on metal oxide nanocrystal sensitized graphite nanoelectrodes through preferential molecular adsorption, J. ElectroAnal. Chem. 867 (2020) 114190, https://doi.org/10.1016/j.jelechem.2020.114190.
[35] J.A. Rodríguez-Manzo, O. Cretu, F. Banhart, Trapping of metal atoms in vacancies of carbon nanotubes and graphene, ACS Nano 4 (6) (2010) 3422–3428, https://doi.org/10.1021/nn100356q.
[36] S. Song, S. Jiang, Selective catalytic oxidation of ammonia to nitrogen over CuO/CNTs: The promoting effect of the defects of CNTs on the catalytic activity and selectivity, Appl. Catal. B 117–118 (2012) 346–350, https://doi.org/10.1016/j.apcatb.2012.01.030.
[37] B. Mehdizadeh, L. Maleknia, A. Amirabadi, M. Shabani, Glucose sensing by a glassy carbon electrode modified with glucose oxidase/chitosan/graphene oxide nanofibers, Diam. Relat. Mater. 109 (2020) 108073, https://doi.org/10.1016/j.diamond.2020.108073.
[38] S. Guo, P. Yu, W. Li, Y. Yi, F. Wu, L. Mao, Electron hopping by interfacing semiconducting graphdiyne nanosheets and redox molecules for selective electrocatalysis, J. Am. Chem. Soc. 142 (4) (2020) 2074–2082, https://doi.org/10.1021/jacs.9b13678.
[39] M. Briones, E. Casero, M.D. Petit-Domínguez, M.A. Ruiz, A.M. Parra-Alfambra, F. Pariente, E. Lorenzo, L. Vázquez, Diamond nanoparticles based biosensors for efficient glucose and lactate determination, Biosens. Bioelectron. 68 (2015) 521–528, https://doi.org/10.1016/j.bios.2015.01.044.
[40] A. Jędrzak, T. Rębiś, M. Kuznowicz, T. Jesionowski, Bio-inspired magnetite/lignin/polydopamine-glucose oxidase biosensing nanoplatform. from synthesis, via sensing assays to comparison with others glucose testing techniques, Int. J. Biol. Macromol. 127 (2019) 677–682, https://doi.org/10.1016/j.ijbiomac.2019.02.008.
[41] A. Jędrzak, T. Rębiś, M. Kuznowicz, A. Kołodziejczak-Radzimska, J. Zdarta, A. Piasecki, T. Jesionowski, Microplatforms for glucose oxidase immobilization: evaluation of biosensing properties by catalytic glucose oxidation, Catalysts 9 (2019) 1–19, https://doi.org/10.3390/catal9121044.
[42] S.H. Lim, J. Wei, J. Lin, Q. Li, J. KuaYou, A glucose biosensor based on electrodeposition of palladium nanoparticles and glucose oxidase onto Nafion-solubilized carbon nanotube electrode, Biosens. Bioelectron. 20 (2005) 2341–2346, https://doi.org/10.1016/j.bios.2004.08.005.
[43] S. Huang, Y.u. Ding, Y. Liu, L. Su, R. Filosa, Y.u. Lei, Glucose biosensor using glucose oxidase and electrospun Mn_2O_3-Ag nanofibers, Electroanalysis 23 (8) (2011) 1912–1920, https://doi.org/10.1002/elan.201100221.
[44] M. Artigues, J. Gilabert-Porres, R. Texidó, S. Borrós, J. Abellà, S. Colominas, Analytical parameters of a novel glucose biosensor based on grafted PFM as a covalent immobilization technique, Sensors 21 (2021) 4185, https://doi.org/10.3390/s21124185.
[45] H. Tang, J. Chen, S. Yao, L. Nie, G. Deng, Y. Kuang, Amperometric glucose biosensor based on adsorption of glucose oxidase at platinum nanoparticle-modified carbon nanotube electrode, Anal. Biochem. 331 (1) (2004) 89–97, https://doi.org/10.1016/j.ab.2004.05.005.
[46] F. Jiménez-Fiérrez, M.I. González-Sánchez, R. Jiménez-Pérez, J. Iniesta, E. Valero, Glucose biosensor based on disposable activated carbon electrodes modified with platinum nanoparticles electrodeposited on poly(Azure a), Sensors 20 (2020) 1–15, https://doi.org/10.3390/s20164489.
[47] A. Márquez, C. Jiménez-Jorquera, C. Domínguez, X. Muñoz-Berbel, Electrodepositable alginate membranes for enzymatic sensors: An amperometric glucose biosensor for whole blood analysis, Biosens. Bioelectron. 97 (2017) 136–142, https://doi.org/10.1016/j.bios.2017.05.051.
[48] O. Sadak, A.K. Sundramoorthy, S. Gunasekaran, Highly selective colorimetric and electrochemical sensing of iron(III) using Nile red functionalized graphene film, Biosens. Bioelectron. 89 (2017) 430–436, https://doi.org/10.1016/j.bios.2016.04.073.
[49] C. Nan, Y. Zhang, G. Zhang, C. Dong, S. Shuang, M.M.F. Choi, Activation of nylon net and its application to a biosensor for determination of glucose in human serum, Enzyme Microb. Technol. 44 (5) (2009) 249–253, https://doi.org/10.1016/j.enzmictec.2008.12.007.
[50] A. Soni, S.K. Jha, Smartphone based non-invasive salivary glucose biosensor, Anal. Chim. Acta 996 (2017) 54–63, https://doi.org/10.1016/j.aca.2017.10.003.
[51] A. Soni, S.K. Jha, A paper strip based non-invasive glucose biosensor for salivary analysis, Biosens. Bioelectron. 67 (2015) 763–768, https://doi.org/10.1016/j.bios.2014.09.042.
[52] J.R. Anusha, A.T. Fleming, H.J. Kim, B.C. Kim, K.H. Yu, C.J. Raj, Effective immobilization of glucose oxidase on chitosan submicron particles from gladius of Todarodes pacificus for glucose sensing, Bioelectrochemistry 104 (2015) 44–50, https://doi.org/10.1016/j.bioelechem.2015.02.004.
[53] X. Kang, J. Wang, H. Wu, I.A. Aksay, J. Liu, Y. Lin, Glucose Oxidase-graphene-chitosan modified electrode for direct electrochemistry and glucose sensing, Biosens. Bioelectron. 25 (4) (2009) 901–905, https://doi.org/10.1016/j.bios.2009.09.004.
[54] K. Wang, Q. Liu, Q.-M. Guan, J. Wu, H.-N. Li, J.-J. Yan, Enhanced direct electrochemistry of glucose oxidase and biosensing for glucose via synergy effect of graphene and CdS nanocrystals, Biosens. Bioelectron. 26 (2011) 2252–2257, https://doi.org/10.1016/j.bios.2010.09.043.
[55] M. Baghayeri, H. Veisi, M. Ghanei-Motlagh, Amperometric glucose biosensor based on immobilization of glucose oxidase on a magnetic glassy carbon electrode modified with a novel magnetic nanocomposite, Sens. Actuators B Chem. 249 (2017) 321–330, https://doi.org/10.1016/j.snb.2017.04.100.
[56] R.B. Rakhi, P. Nayuk, C. Xia, H.N. Alshareef, Novel amperometric glucose biosensor based on MXene nanocomposite, Sci. Rep. 6 (2016) 36422, https://doi.org/10.1038/srep36422.
[57] H. Zhang, Z. Meng, Q.i. Wang, J. Zheng, A novel glucose biosensor based on direct electrochemistry of glucose oxidase incorporated in biomediated gold nanoparticles-carbon nanotubes composite film, Sens. Actuators B Chem. 158 (1) (2011) 23–27, https://doi.org/10.1016/j.snb.2011.04.057.
[58] S. Khumngern, R. Jirakunakorn, P. Thavarungkul, P. Kanatharana, A. Numnuam, A highly sensitive flow injection amperometric glucose biosensor using a gold nanoparticles/polytyramine/Prussian blue modified screen-printed carbon electrode, Bioelectrochemistry 138 (2021) 107718, https://doi.org/10.1016/j.bioelechem.2020.107718.
[59] Y. Liu, X.u. Nan, W. Shi, X. Liu, Z.i. He, Y. Sun, D. Ge, A glucose biosensor based on the immobilization of glucose oxidase and Au nanocomposites with polynorepinephrine, RSC Adv. 9 (29) (2019) 16439–16446, https://doi.org/10.1039/c9ra02054c.
[60] A. Umar, M.M. Rahman, S.H. Kim, Y.B. Hahn, ZnO nanonails: Synthesis and their application as glucose biosensor, J. Nanosci. Nanotechnol. 8 (6) (2008) 3216–3221, https://doi.org/10.1166/jnn.2008.116.
[61] H. Bisswanger, Enzyme assays, Perspect Sci. 1 (1-6) (2014) 41–55, https://doi.org/10.1016/j.pisc.2014.02.005.
[62] S. Donmez, F. Arslan, N. Sarı, E. Hasanoğlu Özkan, H. Arslan, Glucose biosensor based on immobilization of glucose oxidase on a carbon paste electrode modified with microsphere-attached l-glycine, Biotechnol. Appl. Biochem. 64 (2017) 745–753, https://doi.org/10.1002/bab.1533.
[63] N. Demirkiran, E. Ekinci, M. Asiltürk, Immobilization of glucose oxidase in silica sol-gel film for application to biosensor and amperometric determination of glucose, J. Chil. Chem. Soc. 57 (2012) 1336–11139, https://doi.org/10.4067/S0717-97072012000400001.
[64] P. Panjan, V. Virtanen, A.M. Sesay, Determination of stability characteristics for electrochemical biosensors via thermally accelerated ageing, Talanta 170 (2017) 331–336, https://doi.org/10.1016/j.talanta.2017.04.011.